

Molecular Dynamics Analysis on Effects of Vacancies upon Mechanical Properties of Graphene and Graphite

Akihiko Ito and Shingo Okamoto

Abstract—The mechanical properties of graphene and graphite containing vacancies under tensile loading were investigated using molecular dynamics simulations. Two types of potential functions were used in the simulations: the second-generation reactive empirical bond-order (REBO) potential for covalent C–C bonds, and the Lennard-Jones potential for the interlayer interaction in graphite. The influence of the size and distribution of the vacancies on the mechanical properties of graphene and graphite were studied. It was found that the tensile strengths of graphene and graphite are significantly decreased when they contain randomly distributed vacancies.

Index Terms—Graphene, graphite, molecular dynamics, vacancy

I. INTRODUCTION

CARBON-based materials can have excellent mechanical and electrical properties. Consequently, their application to structural subassemblies and nanoelectromechanical systems such as electrochemical electrodes and field emission has attracted considerable interest. Carbon materials such as diamond, graphene, carbon nanotubes (CNTs), and fullerenes have a wide range of excellent properties thanks to the different types of bonds and atomistic structures contained within them. In particular, graphene has rigidity and strength almost on a par to that of diamond, as well as novel electronic properties that include high electron mobility. Thus, the study of graphene and graphite made of graphene layers has recently intensified [1]–[3].

Defects often affect the mechanical and electronic properties of materials. There have been reports of experimental studies on defects (i.e., vacancies [4], dislocations [5], and grain boundaries [6]) in graphene layers. It is important to clarify the influence of defects on the mechanical and electrical properties of graphene and graphite

in order to produce high-performance carbon materials.

Studies aiming to clarify the relationship between atomic-scale defects and mechanical properties have recently increased in number. For example, the tensile properties of graphene and CNTs containing multiple Stone-Wales (SW) defects have been investigated using molecular dynamics (MD) simulations by Xiao *et al.* [7]. Such studies have clarified the relationship between the number of defects present and the mechanical properties of a system. The influence of grain boundaries on the tensile strength of graphene has been investigated by Grantab *et al.* [8], while MD simulations on the tensile loadings of single-walled CNTs with vacancies have been performed by Wong *et al.* [9]. The influence of single and double vacancies on the tensile strength has been investigated through molecular mechanics (MM) calculations by Zhang *et al.* [10]. Zhang *et al.* compared their results obtained using MM calculations to those obtained by Mielke using quantum mechanics (QM) calculations [11]. However, the influence of vacancies on the mechanical properties of graphene and graphite has yet to be fully clarified. Recently, we elucidated the effect of vacancy size on the mechanical properties of graphene through MD simulations [12]. In the present study, we also investigate the effects of the size and distributional form of vacancies in graphite on these same properties.

II. METHOD

A. Potential Functions

In the present study, we used two types of interatomic potential: the second-generation reactive empirical bond order (2nd REBO) [13] and Lennard-Jones potentials. The 2nd REBO potential for covalent C–C bonds is expressed as

$$E_{REBO} = \sum_i \sum_{j>i} [V_R(r_{ij}) - B_{ij}^* V_A(r_{ij})], \quad (1)$$

where r_{ij} represents the distance between atoms i and j . The B_{ij}^* represents the bond-order term. The terms $V_R(r_{ij})$ and $V_A(r_{ij})$ represent the pair-additive interactions that reflect interatomic repulsions and attractions, respectively, as in

Manuscript received May 10, 2012. This work was supported in part by the Ring-Ring project of JKA.

A. Ito is with the Mechanical Engineering Course, Graduate School of Science and Engineering, Ehime University, 3 Bunkyo-cho, Matsuyama 790-8577, Japan. He is also with the Composite Materials Research Laboratories, Toray Industries, Inc., Masaki-cho 791-3193, Japan (e-mail: Akihiko_Ito@nts.toray.co.jp).

S. Okamoto is with the Mechanical Engineering Course, Graduate School of Science and Engineering, Ehime University, 3 Bunkyo-cho, Matsuyama 790-8577, Japan (e-mail: okamoto.shingo.mh@ehime-u.ac.jp).

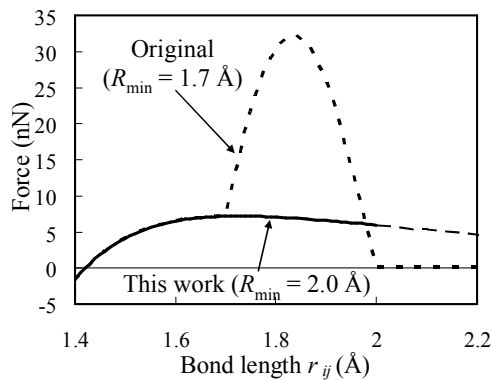


Fig. 1. Interatomic forces for the 2nd REBO potential with original R_{\min} and modified R_{\min} (this work).

$$V_R(r) = f_c(r) \left(1 + \frac{Q}{r} \right) A \exp(-\alpha r) \quad (2)$$

$$V_A(r) = f_c(r) \sum_{n=1}^3 B_n \exp(-\beta_n r)$$

where Q , A , α , B_n , and β_n represent constants. The function $f_c(r)$ represents the cutoff function that decreases monotonously from 1 to 0 as in

$$f_c(r) = \begin{cases} 1, & r < R_{\min} \\ \left\{ 1 + \cos \left[\frac{\pi(r - R_{\min})}{R_{\max} - R_{\min}} \right] \right\} / 2, & R_{\min} < r < R_{\max} \\ 0, & r > R_{\max} \end{cases} \quad (3)$$

where $R_{\min} = 1.7 \text{ \AA}$ and $R_{\max} = 2.0 \text{ \AA}$ in the original 2nd REBO potential.

It is known that for the original 2nd REBO potential, the interatomic forces increase dramatically at $r = R_{\min}$ and reach zero at $r = R_{\max}$ because of the discontinuity in the second derivative of the cutoff function, as shown in Fig. 1. This dramatic increase in the interatomic force with the original 2nd REBO potential may greatly affect the tensile strength. Therefore, in this work, the cutoff parameter was set to 2.0 \AA to avoid any dramatic increase in the interatomic force [14]. The other parameters, except for R_{\min} , were set to the values proposed by Brenner [13]. The Lennard-Jones potential for the interlayer interaction in the graphite model is expressed as

$$V^{LJ} = 4\epsilon \left[\left(\frac{r_0}{r_{ij}} \right)^{12} - \left(\frac{r_0}{r_{ij}} \right)^6 \right] \quad (4)$$

The use of the 2nd REBO potential and Lennard-Jones potential are switched according to the interatomic distance and bond order [15]. The value of ϵ was set to 0.00284 eV and r_0 was set to 3.2786 \AA so that the interplanar spacing in graphite at 300 K is 3.35 \AA , which is a known experimental value [16].

B. Analysis Model

Two types of graphene models, referred to as zigzag graphene (ZGR) and armchair graphene (AGR) models, are

used according to the tensile directions. The analysis models of perfect ZGR and AGR consist of 588 and 576 carbon atoms, respectively, with dimensions equal to those of a real crystallite in a typical carbon material, as shown in Fig. 2.

No periodic boundary conditions are imposed in our case and the analysis models consist of two parts. The first is referred to as

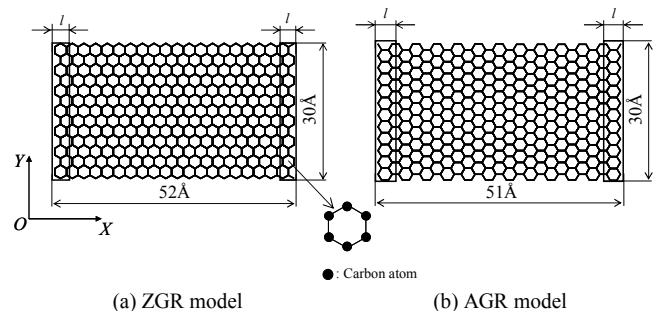


Fig. 2. Configurations of graphene used under zigzag and armchair tension. ZGR: Zigzag graphene, AGR: Armchair graphene

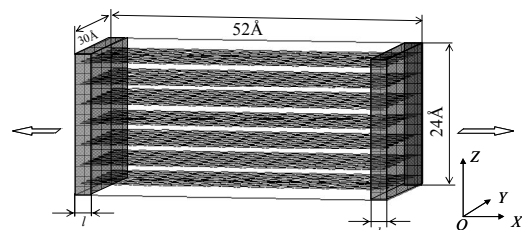


Fig. 3. Configuration of graphite used under zigzag tension in the X direction.

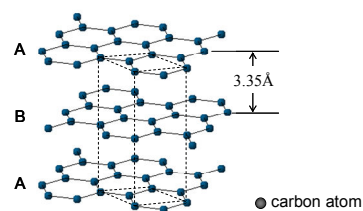


Fig. 4. Schematic of the structure of graphite, with the interlayer spacing shown.

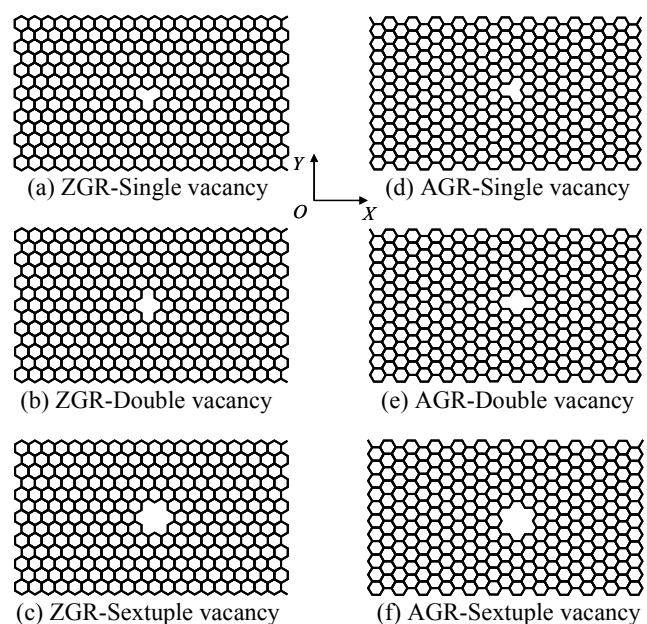


Fig. 5. Analysis models for graphene containing cluster-type vacancies. ZGR: Zigzag graphene, AGR: Armchair graphene

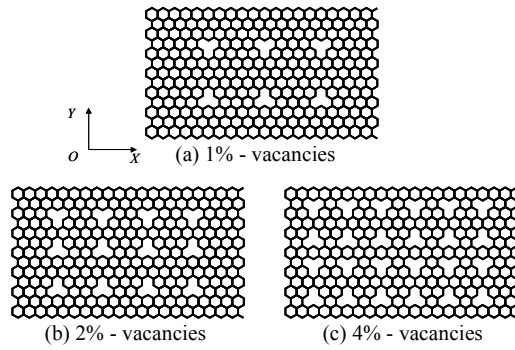


Fig. 6. Analysis models for the ZGR (zigzag graphene) containing uniformly distributed vacancies.

the active zone in which the atoms move according to the interactions with their neighboring atoms. The other—enclosed within the boxes shown in Fig. 2—is referred to as the boundary zone in which the atoms are constrained. The thickness, l , of the boundary zone is $3.0a$ for the AGR model and $1.5 \times \sqrt{3}a$ for the ZGR model, where a is the length of the C=C bond in graphene.

The analysis model of perfect graphite used under zigzag tension in the X direction, consists of 4,116 carbon atoms, with dimensions equal to those of a real crystallite of a typical carbon material, as shown in Fig. 3. The graphite model is made of seven layers of graphene sheets that are stacked in an AB-type sequence with an interlayer spacing of 3.35 \AA , as shown in Fig. 4.

We conducted two investigations on the effects of vacancies. The first is on the size of the vacancy. The analysis models used of graphene with cluster-type vacancies are shown in Fig. 5. These models of graphite reveal that the ZGR sheet with a cluster-type vacancy is always the central layer.

The distributional form of the vacancy is also investigated using the ZGR model. The analysis models of the ZGR containing uniformly distributed vacancies are shown in Fig. 6. Each vacancy is a single vacancy, set so that the distance between neighboring vacancies is identical. Calculations for three values of vacancy density, namely 1, 2, and 4%, were performed. The analysis models of graphite with 1, 2, and 4% vacancies were constructed using seven layers of the ZGR model with the corresponding density of vacancies.

The analysis models of graphene and graphite containing randomly distributed vacancies were set by removing carbon atoms in the active zone by using a pseudorandom number generator.

C. Molecular Dynamics Simulations

We investigated the mechanical properties of vacancy-containing graphene and graphite using MD simulations under constant volume and temperature, i.e., a canonical (NVT) ensemble. The equations of motion of the atoms were time-integrated using the velocity Verlet method. The velocities of all atoms were adjusted simultaneously using the velocity scaling method [17] so that the temperature of the object was maintained at the preset temperature, T_{SET} . The mass of a single carbon atom, m , is $1.9927 \times 10^{-26} \text{ kg}$. The time step used was 1.0 fs .

The atomic stress acting on each atom was calculated to obtain the stress-strain curves and to visualize the stress

distribution during tensile loadings. The atomic stress, σ_J^i , for each of the X , Y , and Z directions of J is given by calculating the kinetic energies of, the interatomic force acting on, and the volume occupied by atom i , as in

$$\sigma_J^i = \frac{1}{\Omega^i} \left(m \overline{V^i J V^i J} + \overline{J^i F^i J} \right), \quad (5)$$

where Ω^i represents the volume occupied by atom i , which is referred to as the atomic volume. The atomic volume is calculated by averaging the volume over all atoms in the initial structure of each system. The interatomic force acting on atom i due to its neighboring atoms is represented by F^i . The global stress of an analysis model can then be calculated by averaging over all carbon atoms in each system.

Method of Tension Loading

The initial positions of the atoms were such that the analysis model represents the crystal structure of graphene or graphite at a preset temperature. First, the atoms in the active zone of the analysis model were relaxed in unloaded states for 7,000 MD steps. The atoms in the boundary zone were then fixed in all directions for the graphene models and in only the X and Y directions for the graphite models. After constant displacements were applied to the atoms in both of the boundary zones to simulate uniaxial tensile loading in the X direction, the atoms in the active zone were relaxed for 7,000 MD steps. The strain increment used, $\Delta \epsilon$, was 0.004. The output stresses were sampled for the last 2,000 MD steps for each strain and then averaged. Young's moduli were obtained from the slopes of the straight lines in the range where the relationship between the stress and strain is linear, and tensile strengths are given by the last peak of the nominal stress-nominal strain curves.

III. RESULTS AND DISCUSSION

A. Validation of Calculation Method

We performed MD simulations on the tensile loadings of pristine zigzag graphene (p-ZGR) and pristine armchair graphene (p-AGR) at 300 K to verify the validity of our calculation method. The results are presented in Table I and Fig. 7. An average tensile strength of 83 GPa was obtained, which is in close agreement with the 121 GPa calculated by Pei *et al.* through MD simulations [18] and with the experimentally obtained value of 123.5 GPa [1]. The average Young's modulus of 836 GPa is within the range of results encompassed by those obtained by density functional theory [19] (1,050 GPa) and by experiment [20] (500 GPa and 1 TPa). It is estimated that the lower value obtained in this work

TABLE I
MECHANICAL PROPERTIES OF PRISTINE GRAPHENE

| Material | Tensile strength (GPa) | Young's modulus (GPa) |
|----------|------------------------|-----------------------|
| p-AGR | 76 | 879 |
| p-ZGR | 91 | 794 |
| Average | 83 | 836 |

p-AGR: pristine armchair graphene, p-ZGR: pristine zigzag graphene.

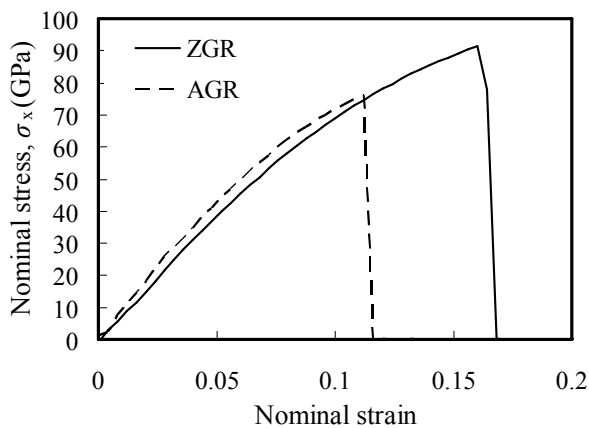


Fig. 7. Stress-strain curves of pristine graphene under Armchair or Zigzag tension.

is due to the effect of model size on the elastic properties of graphene [20].

B. Effect of Vacancy Size on Mechanical Properties of Graphene

The mechanical properties of vacancy-containing zigzag graphene (v-ZGR) and vacancy-containing armchair graphene (v-AGR) obtained at 300 K are listed in Tables II to IV, together with the results from previous studies on CNTs [9]–[11]. The nominal stress-nominal strain curves for the v-ZGR and v-AGR are given in Figs. 8 and 9, respectively. The results for pristine graphene are also provided for reference.

For the v-ZGR, the decrease in tensile strength is largest for graphene with a double vacancy, followed by that for the sextuple, and then single vacancy species. In addition, the fracture strain for graphene with a double vacancy is the least of those studied. The decrease in tensile strength relative to that of pristine graphene is 29, 28, and 17% for the double, sextuple, and single v-ZGR, respectively.

For the v-AGR, the decrease in tensile strength is largest for graphene with a sextuple vacancy, followed by the single then double vacancy v-AGR. The decrease in tensile strength relative to that of pristine graphene is 32, 19, and 18% for the sextuple, single, and double vacancy v-AGR, respectively.

Compared with the results of previous studies on CNTs using MD [9], MM [10], and QM [11] calculations, the reductions in the tensile strength of the v-ZGR and v-AGR with a single and double vacancy in this work are similar to those obtained with the MM and QM calculations and not close to those obtained previously by MD calculations.

For both the v-ZGR and the v-AGR, the Young's modulus shows no significant change with the change in vacancy size.

Snapshots of the tensile loadings of the ZGR and AGR are shown in Figs. 10 and 11, respectively. For the p-ZGR (Fig. 10(a-2)), the distribution of stress immediately before fracture is uniform and the level of stress is high. In comparison, in the v-ZGR, the majority of the stress occurs around the vacancy just before fracture, which emerges from the circumference of the vacancy. For all cases of AGR (Fig. 11), the fractures progress perpendicular to the tensile axis.

We compared the calculated results with the Griffith's

TABLE II
TENSILE STRENGTHS OF VACANCY-CONTAINING ZGR AND [5,5] CNT

| Material | ZGR | [5,5] CNT(Carbon Nanotube) | | |
|---------------|-------------------------|-----------------------------|------------------------------|------------------------------|
| | σ_B (MD, GPa) | σ_B [9] (MD, GPa) | σ_B [10] (MM, GPa) | σ_B [11] (QM, GPa) |
| Pristine | 91 | 104 | 105.5 | 135 |
| Single vac. | 75 (-17%) | 103 (-1%) | 70.4 (-33%) | 100 (-26%) |
| Double vac. | 64 (-29%) | 101 (-3%) | 71.3 (-32%) | 105 (-22%) |
| Sextuple vac. | 65 (-28%) | — | — | — |

σ_B is the tensile strength. Values in parentheses represent the differences between the pristine and vacancy-containing materials. MD, MM, and QM refer to Molecular Dynamics, Molecular Mechanics, and Quantum Mechanics, respectively.

TABLE III
TENSILE STRENGTHS OF VACANCY-CONTAINING AGR AND [10,0] CNT

| Material | AGR | [10,0] CNT(Carbon Nanotube) | | |
|---------------|-------------------------|-----------------------------|------------------------------|------------------------------|
| | σ_B (MD, GPa) | σ_B [9] (MD, GPa) | σ_B [10] (MM, GPa) | σ_B [11] (QM, GPa) |
| Pristine | 76 | 90 | 87.9 | 124 |
| Single vac. | 61 (-19%) | — | 64.8 (-26%) | 101 (-18%) |
| Double vac. | 62 (-18%) | 85 (-5.5%) | 64.4 (-26%) | 107 (-13%) |
| Sextuple vac. | 51 (-32%) | — | — | — |

σ_B is the tensile strength. Values in parentheses represent the differences between the pristine and vacancy-containing materials. MD, MM, and QM refer to Molecular Dynamics, Molecular Mechanics, and Quantum Mechanics, respectively.

TABLE IV
THE YOUNG'S MODULI OF VACANCY-CONTAINING GRAPHENE (UNIT: GPa)

| Material | ZGR | AGR |
|------------------|-------------|-------------|
| Pristine | 794 | 879 |
| Single vacancy | 782 (-1.5%) | 868 (-1.2%) |
| Double vacancy | 765 (-3.6%) | 870 (-1.0%) |
| Sextuple vacancy | 767 (-3.4%) | 848 (-3.6%) |

Values in parentheses represent the differences between the pristine and vacancy-containing materials.

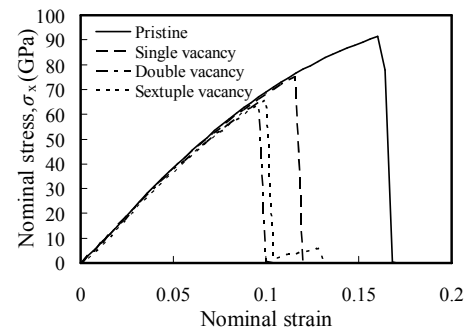


Fig. 8. Stress-strain curves of ZGR (zigzag graphene) containing a cluster-type vacancy under zigzag tension.

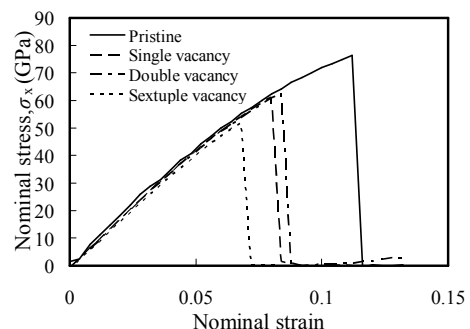


Fig. 9. Stress-strain curves of the AGR (armchair graphene) containing a cluster-type vacancy under zigzag tension.

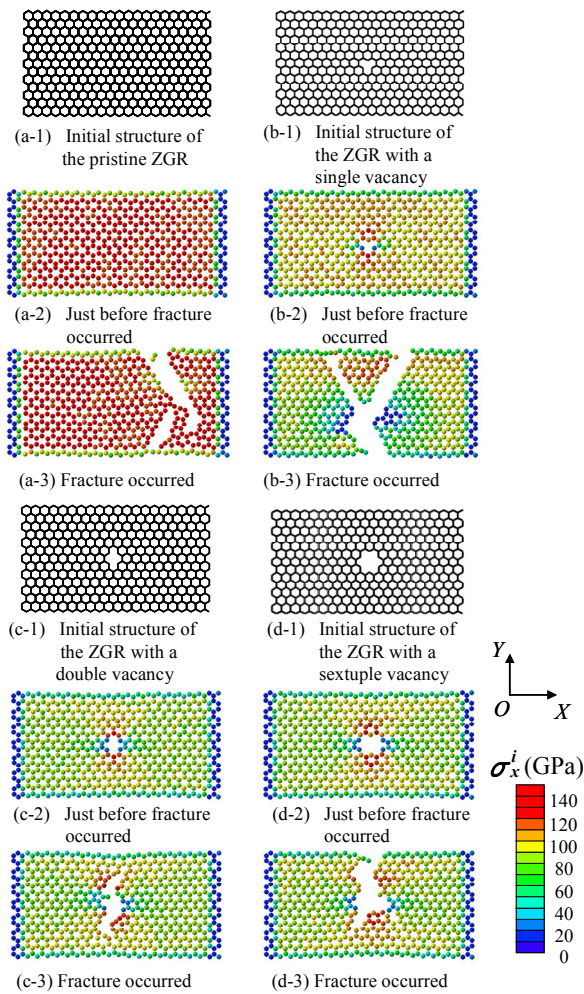


Fig. 10. Stages of fracture progression in the ZGR (zigzag graphene) containing cluster-type vacancies. (a-1)–(a-3): pristine, (b-1)–(b-3): single vacancy, (c-1)–(c-3): double vacancy, and (d-1)–(d-3): sextuple vacancy.

criterion in order to verify their validity. The theoretically ideal strength σ_{\max} for brittle fracture is expressed as

$$\sigma_{\max} = \sqrt{\frac{E\gamma_s}{d}}, \quad (6)$$

where E is Young's modulus, γ_s is the surface energy, and d is the interatomic distance. Consequently, according to the Griffith's criterion, the strength of a material containing a crack of length $2C$ is expressed as

$$\sigma_f = \sqrt{\frac{2E\gamma_s}{\pi C}}. \quad (7)$$

The relative strength, σ_{rel} , i.e., the strength of the crack-containing material relative to the theoretically ideal strength is obtained by dividing σ_f by σ_{\max} as

$$\sigma_{\text{rel}} = \sqrt{\frac{2d}{\pi C}}. \quad (8)$$

A plot of the relative strength of the ZGR and AGR against

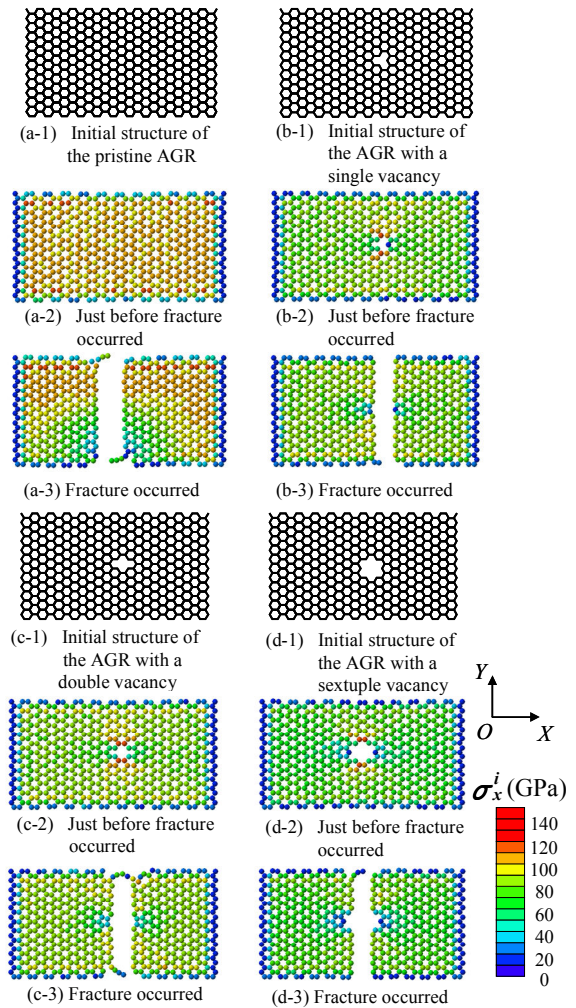


Fig. 11. Stages of fracture progression in the AGR (armchair graphene) containing cluster-type vacancy. (a-1)–(a-3): pristine, (b-1)–(b-3): single vacancy, (c-1)–(c-3): double vacancy, and (d-1)–(d-3): sextuple vacancy.

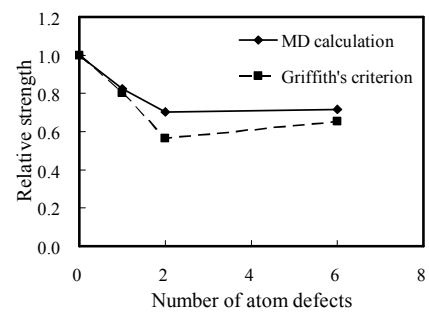


Fig. 12. Relative strengths and sizes of vacancy, i.e., the number of atom defects in the zigzag graphene (ZGR) obtained using MD and Griffith's criterion.

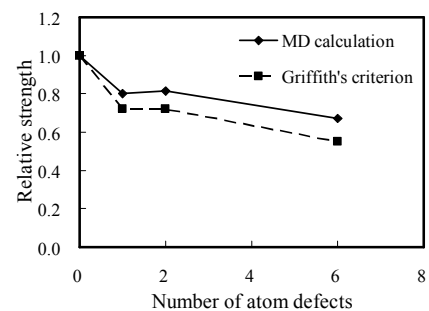


Fig. 13. Relative strengths and sizes of vacancy, i.e., the number of atom defects in the armchair graphene (AGR) obtained using MD and Griffith's criterion.

the number of atomic defects is shown in Figs. 12 and 13, respectively. The results of the MD calculations agree well with the predicted values using Griffith's criterion for both the ZGR and AGR.

C. Effect of Vacancy Size on Mechanical Properties of a Graphene Sheet in Graphite

The mechanical properties of a vacancy-containing graphene sheet in graphite are listed in Table V. The stress-strain curves of the graphite are given in Fig. 14. The results for pristine graphite are also provided for reference. In every case, reductions in stress occur before the fracture.

For the cluster-type vacancy, the tensile strengths of the central layer in the graphite and the graphene are shown in Fig. 15. For all types of vacancy studied, the tensile strength of the central layer is almost equal to that of graphene with a similarly sized vacancy. This means that the interlayer interaction has negligible effect on the tensile strength of the vacancy-containing central layer.

Snapshots of the graphite with a sextuple vacancy are shown in Fig. 16. It was found that the reduction in stress before fracture was due to a tear in the graphene sheet. For the

TABLE V
MECHANICAL PROPERTIES OF VACANCY-CONTAINING GRAPHITE

| Material | σ_B (GPa) | E (GPa) |
|------------------|---------------------|--------------|
| Pristine | 91 | 816 |
| Single vacancy | 78 (-14%) | 815 (-0.1%) |
| Double vacancy | 65 (-28%) | 804 (-1.4%) |
| Sextuple vacancy | 70 (-23%) | 788 (-3.4%) |

σ_B is the tensile strength. E is the Young's modulus. Values in parentheses represent the differences between the pristine and vacancy-containing materials.

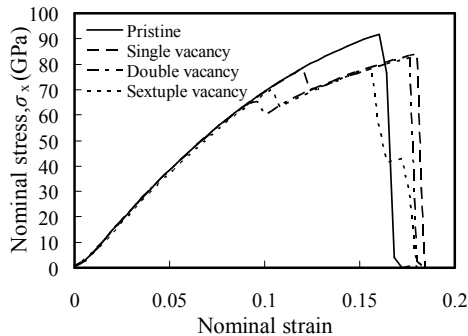


Fig. 14. Stress-strain curves of graphite containing cluster-type vacancies under zigzag tension.

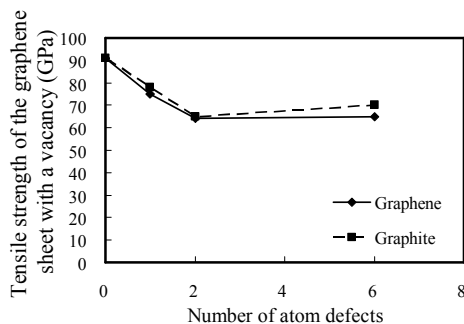


Fig. 15. Tensile strength of graphene with a vacancy and of the vacancy-containing central layer in graphite, which depend on the size of the vacancy, i.e., the number of atomic defects.

sextuple vacancy, the reduction in stress is due to the tearing of the vacancy-containing central layer ((a-1) and (b-1) in Fig. 16). The stress then reached a maximum before the other layers caused fractures. In this case, the atom in the broken piece of the central layer reacts with the atom at the edge of the neighboring layer, leading to the tearing of the neighboring layer by disturbing the zigzag-edge surface (see Fig. 17).

D. Influence of Distributional Form of Vacancies

The relationship between the tensile strength and density of vacancies for both graphene and graphite with uniformly or randomly distributed vacancies is shown in Fig. 18. For the randomly distributed vacancies, the average values of the two results calculated using the models with different vacancy arrangements is plotted. The error bar in the graph represents the range between these two values. There is no difference in the tensile strength of graphene and graphite. The tensile strength decreases with an increase in vacancy density. The reduction in the tensile strength stands at about 60% for a vacancy density of 4% with the random vacancy distribution. This is nearly double the reduction observed for the tensile strength of hydrogen (H)-functionalized graphene [18]. In comparison, the Young's modulus slightly decreases with the increase in vacancy density for both graphene and graphite (see Fig. 19). The reduction in the Young's modulus is about 20% for a vacancy density of 4%. This is nearly 4 times greater than the reduction in Young's modulus previously determined for H-functionalized graphene. It is therefore reasonable to assume that the properties of graphene and graphite are more sensitive to vacancies than to H-coverage, since whereas a vacancy implies the lack of an atom, H-coverage refers to the conversion of local carbon bonding

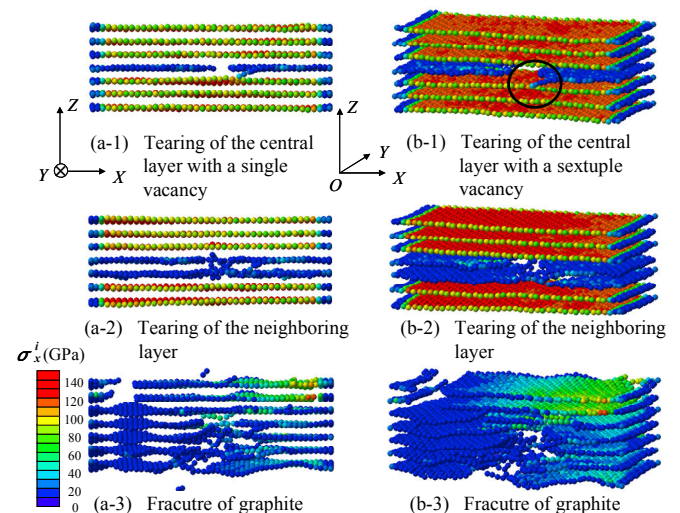


Fig. 16. Stages of fracture progression of graphite with a sextuple vacancy ((a-1)–(a-3): viewed in the Y direction, (b-1)–(b-3): viewed in the direction of slant.)

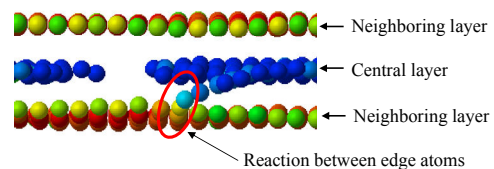


Fig. 17. Enlargement of the circled section shown in Fig. 16(b-1).

from sp^2 to sp^3 hybridization.

Snapshots of the graphene with uniformly distributed vacancies during tensile loading are shown in Fig. 20. For every case studied herein, the majority of the stress occurs around each vacancy just before the fracture, in the same manner witnessed for the graphene with a single vacancy. Fractures then occur, starting from a vacancy and progressing towards neighboring vacancies. The progression direction of the fracture is perpendicular to the tensile axis in all cases. Conversely, the snapshots of graphene with randomly distributed vacancies during the tensile loading (Fig. 21) show that the fracture starts from the area where the vacancies gather. Thereafter, the progression direction of the fracture is then random.

IV. CONCLUSION

We performed MD simulations of tensile loadings on vacancy-containing graphene and graphite to investigate the influence of vacancies on their mechanical properties. It was found that for cluster-type vacancies, the relationship between the size of the vacancy and the tensile strength agree with the relationship predicted using Griffith's criterion.

We demonstrated that the difference in the distributional form of the vacancies affects the tensile strength. In addition, no significant difference was found between the tensile strengths of vacancy-containing graphene and of a graphene sheet in graphite containing a similarly sized vacancy. For the uniformly or randomly distributed vacancies, there is little difference in the tensile strengths between graphene and graphite.

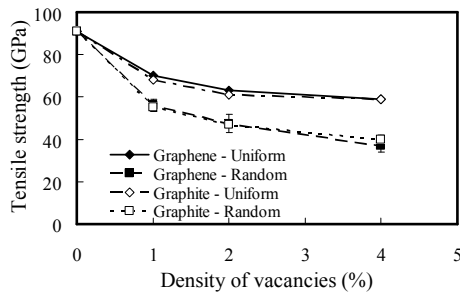


Fig. 18. Tensile strengths of graphene and graphite against vacancy density. Error bars illustrate the range used to calculate the average strengths shown.

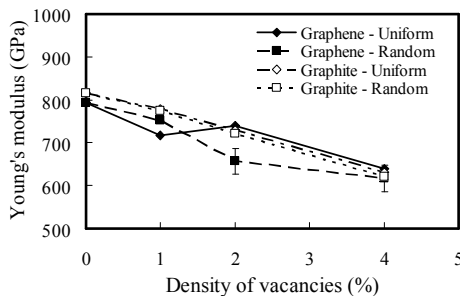


Fig. 19. Young's moduli of graphene and graphite against vacancy density. Error bars illustrate the range used to calculate the average moduli shown.

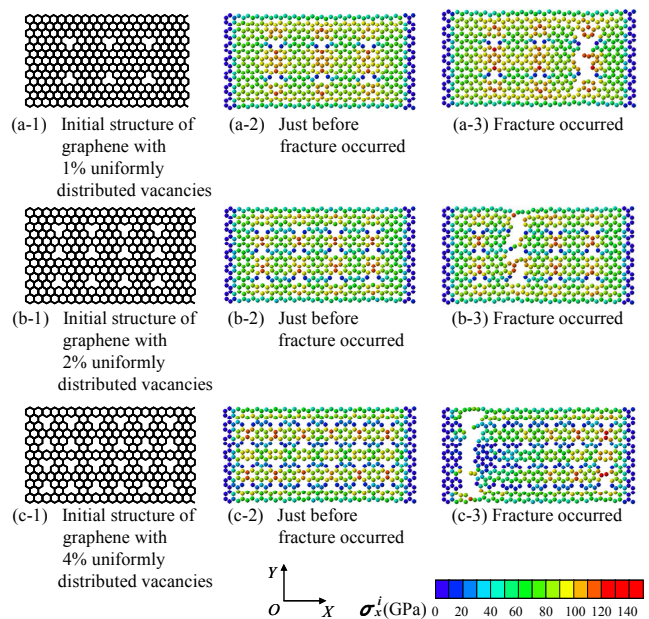


Fig. 20. Stages of fracture progression in graphene containing uniformly distributed vacancies. The density of vacancies is 1% ((a-1)–(a-3)), 2% ((b-1)–(b-3)), and 4% ((c-1)–(c-3)).

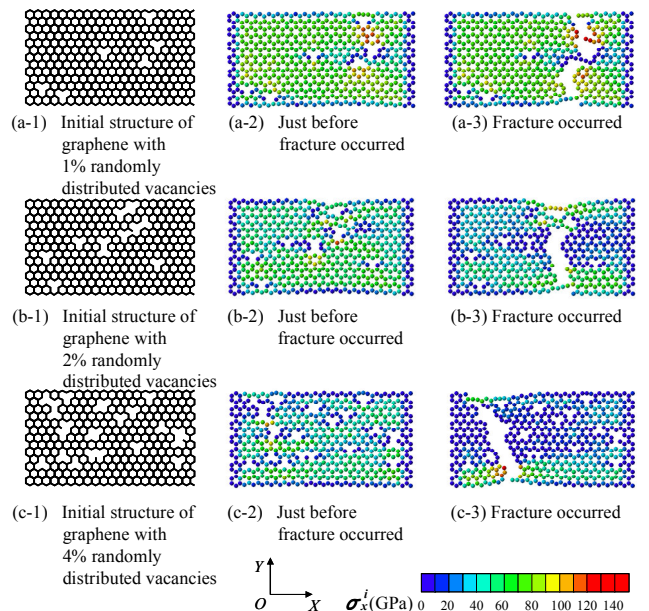


Fig. 21. Stages of fracture progression in graphene containing randomly distributed vacancies. The density of vacancies is 1% ((a-1)–(a-3)), 2% ((b-1)–(b-3)), and 4% ((c-1)–(c-3)).

REFERENCES

- [1] C. Lee, X. Wei, J. W. Kysar, and J. Hone, "Measurement of the elastic properties and intrinsic strength of monolayer graphene," *Science*, vol. 321, pp. 385–388, Jul. 2008.
- [2] H.-L. Zhang, S.-F. Wang, R. Wang, and J. Jiao, "The dislocations in graphene with the correction from lattice effect," *Eur. Phys. J. B*, vol. 73, pp. 489–493, Feb. 2010.
- [3] S. K. Georgantinos, G. I. Giannopoulos, and N. K. Anifantis, "Numerical investigation of elastic mechanical properties of graphene structures," *Mater. Design*, vol. 31, pp. 4646–4654, Dec. 2010.
- [4] P. A. Throver, "The study of defects in graphite by transmission electron microscopy," *Chem. Phys. Carbon*, vol. 5, pp. 217, 1969.
- [5] A. Hashimoto, K. Suenaga, A. Gloter, K. Urita, and S. Iijima, "Direct evidence for atomic defects in graphene layers," *Nature*, vol. 430, pp. 870–873, Aug. 2004.
- [6] J. Osing and I. V. Shvets, "Bulk defects in graphite observed with a scanning tunnelling microscope," *Surf. Sci.*, vol. 417, pp. 145–150, Nov. 1998.

- [7] J. R. Xiao, J. Staniszewski, and J. W. Gillespie, Jr., "Tensile behaviors of graphene sheets and carbon nanotubes with multiple Stone-Wales defects," *Mater. Sci. Eng. A*, vol. 527, pp. 715–723, Jan. 2010.
- [8] R. Grantab, V. B. Shenoy, R. S. Ruoff, "Anomalous strength characteristics of tilt grain boundaries in graphene," *Science*, vol. 330, pp. 946–948, Nov. 2010.
- [9] C. H. Wong, "Elastic properties of imperfect single-walled carbon nanotubes under axial tension," *Comp. Mater. Sci.*, vol. 49, pp. 143–147, Jun. 2010.
- [10] S. Zhang, S. L. Mielke, R. Khare, D. Troya, R. S. Ruoff, G. C. Schatz, and T. Belytschko, "Mechanics of defects in carbon nanotubes: atomistic and multiscale simulations," *Phys. Rev. B*, vol. 71, pp. 115403, Mar. 2005.
- [11] S. L. Mielke, D. Troya, S. Zhang, J-L Li, S. Xiao, R. Car, R. Ruoff, G. C. Schatz, and T. Belytschko, "The role of vacancy defects and holes in the fracture of carbon nanotubes," *Chem. Phys. Lett.*, vol. 390, pp. 413–420, Apr. 2004.
- [12] A. Ito and S. Okamoto, "Mechanical properties of vacancy-containing graphene and graphite using molecular dynamics simulations," *Lecture Notes in Engineering and Computer Science: Proceedings of The International MultiConference of Engineers and Computer Scientists 2012, IMECS 2012*, Hong Kong, March, 14–16, 2012, pp. 320–325.
- [13] D. W. Brenner, O. A. Shenderova, J. A. Harrison, S. J. Stuart, B. Ni, and S. H. Sinnott, "A second-generation reactive empirical bond order (REBO) potential energy expression for hydrocarbons," *J. Phys. Condens. Mat.*, vol. 14, pp. 783–802, Jan. 2002.
- [14] O. A. Shenderova, D. W. Brenner, A. Omeltchenko, X. Su, L. H. Yang, and M. Young, "Atomistic modeling of the fracture of polycrystalline diamond," *Phys. Rev. B*, vol. 61, no. 6, pp. 3877–3888, Feb. 2000.
- [15] S. J. Stuart, A. B. Tutein, and J. A. Harrison, "A reactive potential for hydrocarbons with intermolecular interactions," *J. Chem. Phys.*, vol. 112, no. 14, pp. 6472–6486, Jan. 2000.
- [16] W. Ruland, "X-ray studies on the structure of graphitic carbons," *Acta Cryst.*, vol. 18, pp. 992–996, Jun. 1965.
- [17] L. V. Woodcock, "Isothermal molecular dynamics calculations for liquid salts," *Chem. Phys. Lett.*, vol. 10, pp. 257–261, Aug. 1971.
- [18] Q. X. Pei, Y. W. Zhang, and V. B. Shenoy, "A molecular dynamics study of the mechanical properties of hydrogen functionalized graphene," *Carbon*, vol. 48, pp. 898–904, Mar. 2010.
- [19] F. Liu, P. Ming, and J. Li, "Ab initio calculation of ideal strength and phonon instability of graphene under tension," *Phys. Rev. B*, vol. 76, pp. 064120, Aug. 2007.
- [20] J.-W. Jiang, J.-S. Wang, and B. Li, "Young's modulus of graphene: a molecular dynamics study," *Phys. Rev. B*, vol. 80, pp. 113405, Sep. 2009.